ELSEVIER

Journal of Nuclear Materials 241–243 (1997) 793–798

journal of nuclear materials

Experimental studies of the link between production and penetration of impurity atoms into the plasma edge and the central impurity content in TEXTOR-94

B. Unterberg [a,*], H. Knauf [a], P. Lindner [a], V. Philipps [a], A. Pospieszczyk [a], D. Rusbüldt [a], U. Samm [a], B. Schweer [a], M. Rubel [a,b], T. Tanabe [a,c], Y. Ueda [a,c], M. Wada [a,d]

[a] *Institut für Plasmaphysik, Forschungszentrum Jülich GmbH, Ass. EURATOM-KFA, D-52425 Jülich, Germany*
[b] *Royal Institute of Technology, Physics Department Frescati, Ass. EURATOM-NFR, Frescativagen, Stockholm, Sweden*
[c] *Faculty of Engineering, Osaka University, Suita, Osaka, Japan*
[d] *Department of Electronics, Doshisha University, Tanabe, Kyoto, Japan*

Abstract

Characteristic quantities for impurity release from limiters and the penetration of atoms into the plasma boundary have been determined by optical methods on the tokamak TEXTOR-94. The velocity distribution of neon atoms released from a tungsten limiter has been measured. A drastic increase of fast particles could be observed in comparison to the velocity distribution of neon released from a carbon limiter under comparable conditions. As a result the penetration depth of neon increased by a factor of 1.7. The influence of local electron density and temperature near the limiter has been demonstrated for various species as He, C, Ne, Si and Mo comparing different central electron densities. Both penetration depth and neutral fueling efficiency decrease with increasing density. For high Z materials such as Mo prompt redeposition of singly ionized ions is found to be of major importance. The measured radial profile of the ion source distribution of molybdenum under neutral beam heated conditions has been used to calculate the Mo-density in the plasma center for different line averaged central electron densities $\bar{n}_e$, taking into account both the ionization processes inside and outside the LCFS. The decrease of the calculated Mo-density with $\bar{n}_e$ is in agreement with the experimentally observed variation of the central Mo-density.

Keywords: TEXTOR-94; Limiter; Impurity source; Line emission diagnostics; Particle reflection

1. Introduction

The performance of a future fusion reactor will be significantly determined by impurities such as helium, wall material eroded by plasma–wall interaction and possibly additional impurities injected to exhaust the power by radiation. Three different aspects are important: the production of impurities by different release mechanisms, the penetration of impurity neutrals into the plasma edge and the transport of impurity ions into and inside the confined volume. The aim of this paper is to describe different physical parameters governing the penetration of impurity atoms into the plasma edge. For this purpose we illustrate the importance of the plasma surface interaction processes and the resulting velocity distribution, comparing the recycling of neon at a tungsten and a carbon limiter. We will show the influence of the local electron density and temperature at the edge on the penetration depth and the neutral fueling efficiency for various impurity species. Finally we link plasma edge processes to the central impurity density of molybdenum released from a test limiter, explicitly taking into account the radial distribution of the ion source inside and outside the last closed flux surface.

* Corresponding author. Tel.: +49-02461 614 803; fax: +49-02461 615 452; e-mail: B.Unterberg@kfa-juelich.de.

PII S0022-3115(96)00608-3

2. Ion source distribution and central impurity density

The ion source distribution Q inside and outside the last closed flux surface (LCFS) resulting from electron impact ionization of impurity atoms depends on the velocity distribution of neutrals $f(v_0)$ (determined by the plasma wall interaction processes) and the local ionization rate. Parallel to the ionization processes excitation of atoms and subsequent line radiation occurs, allowing the ion source distribution to be deduced from the line emission ϵ [1]

$$Q(r) = -\frac{\partial}{\partial r}(\Gamma_0) = n_0(r) n_e(r) \langle \sigma v \rangle_{ion}(T_e)$$
$$= \epsilon(r) 4\pi \frac{\langle \sigma v \rangle_{ion}(T_e)}{\langle \sigma v \rangle_{ex}(T_e) b_r} \quad (1)$$

where Γ_0 and n_0 describe flux density and density of neutrals, $\langle \sigma v \rangle_{ion}$ the ionization rate coefficient, $\langle \sigma v \rangle_{ex}$ the excitation rate coefficient and b_r the branching ration of the transition. The penetration depth of neutrals $\lambda_{i0} = \bar{v}_0/(n_e \langle \sigma v \rangle_{ion})$ can be used to characterize the extent of the ion source distribution inside the LCFS. The local neutral flux density is obtained from the integral of the ion source distribution from the radial position r up to the radius where all particles are ionized ($\epsilon = 0$). Accordingly, the neutral density can be expressed with a given velocity distribution $f(v_0)$, which can be measured from the Doppler broadening of line emission of impurity atoms, as

$$n_0(r) = \int_{v_0=0}^{\infty} dv_0 f(v_0) \frac{1}{v_0} \int_r^{r(\epsilon=0)} Q(r') dr' \quad (2)$$

A neutral fueling efficiency can be defined as the ratio between the neutral flux entering the confined volume and the total neutral flux released from the target, describing the probability of neutrals to enter the confined volume.

In a simple diffusion model [2] assuming a δ-like ion source at $r' = a - \lambda_{io}$, where a is the radius of the LCFS, the central impurity density is proportional to λ_{io}/D (D is the diffusion coefficient at the edge) for a given flux into the confined volume. An ion source $Q(r')$ radially distributed inside and outside the LCFS can be considered by means of a Green's function $G(r, r')$ as the solution of the homogeneous continuity equation for the total ion density $\partial n^+/\partial t = -\mathrm{div}\,\Gamma^+$ with a radial ion flux given by $\Gamma^+ = -D\,\partial n^+/\partial r + v n^+$ depending on D and the drift velocity v. $G(r, r')$ for ion sources inside and outside the LCFS is derived in [3]. The resulting central density is written

$$n^+(0) = \int_0^{r_w} dr'\, G(0, r') Q(r') \quad (3)$$

with wall radius r_w, and $G(0, r')$ used following Eq. (18) in [3].

3. Experimental set-up to measure impurity production and penetration on TEXTOR-94

The experiments have been performed on the tokamak TEXTOR-94 with a major radius $R = 1.75$ m and a minor radius $a = 0.46$ m, a toroidal magnetic field $B_T = 2.25$ T and a plasma current $I_P = 350$ kA. The measurements shown below have been carried out using test limiters made of different materials and introduced into the vacuum vessel with the help of a limiter lock system at the bottom of the torus. The limiters are observed from a tangential side view using a spectrometer equipped with an intensified CCD camera as detector which yields spectra of radially resolved line emission in the wavelength range from 200–800 nm. Additionally CCD camera measurements with interference filters are made to analyze the overall 2D spatial distribution of emission in toroidal and radial direction. The spatial resolution of these measurements is about 0.5 mm [4].

The measured radial profiles of line emission of impurity atoms are transferred to the ionization source distribution according to Eq. (1). The profiles of electron temperature (T_e) and density (n_e) profiles necessary for such calculations are obtained by means of a thermal helium

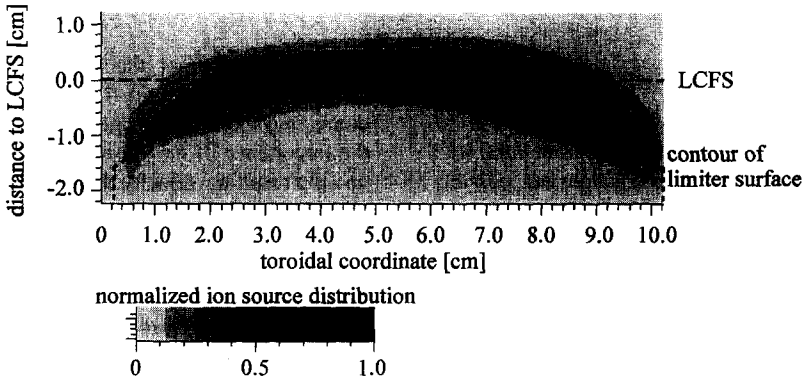

Fig. 1. Normalized ion source distribution of molybdenum deduced from the 2D emission pattern of MoI at 390.3 nm ($r_{lim} = 0.45$ m, $\bar{n}_e = 1.9 \times 10^{19}$ m^{-3}, $P_{heat} = 1.6$ MW).

beam diagnostic [5]. Fig. 1 shows an example of a 2D normalized ion source distribution of molybdenum. Near the limiter the line of sight is oriented tangentially to the magnetic flux surfaces, therefore no unfolding of the measured intensity is necessary. The toroidal axis is oriented horizontally (limiter width 10 cm). The vertical axis refers to the radial direction (LCFS at $y = 0$), negative values correspond to the scrape-off layer (SOL). The limiter is also curved in the poloidal direction and has a poloidal width of 6 cm. The neutral fueling efficiency can be deduced from the ratio between the integral of the ion source inside the LCFS to the total integral. The invisible excitation and ionization processes on the far side of the limiter are assumed to be of equal strength to those at the front side. In a first approximation one can account for the effect of prompt redeposition within the first gyro radius of ions by starting the integration one gyro radius inside the LCFS. The largest uncertainty of the fueling efficiency is given by the position of the LCFS (∓ 1 camera pixel $\Leftrightarrow$ 0.5 mm). With respect to the ionization processes taking place in the SOL we assume that all emission within a circle with a radius $r_l + \rho_L$ corresponds to ions which are promptly reposited, where r_l is the radius of the toroidal curvature of the limiter (indicated as contour in Fig. 1) and ρ_L the larmor radius.

The Doppler broadening of line emission from neutral neon has been measured from the top by guiding the emitted light with fibers to a high resolution ($\lambda/\Delta\lambda = 10^5$) spectrometer [6]. In addition to the Doppler broadening the line shape is determined by the Zeeman-effect. For the NeI transition $3s'[1/2]_{J=1} \rightarrow 3p'[1/2]_{J=0}$ at $\lambda = 585.248$ nm the Zeeman-splitting of the π-component with $\Delta M = 0$ is zero to a first order approximation. This component has been selected by a polarizer. The central molybdenum density has been monitored by soft X-ray emission from L-shell radiation ($\sim$ 2.3–2.9 keV). A collector probe has been positioned in the SOL at a toroidal position 270° away from the limiter lock and analyzed after exposure for the collected amount of Mo.

4. Influence of plasma surface interaction processes: Penetration of neon atoms recycling at carbon and tungsten limiters

Since the target to projectile mass ratio is changing from 12:20 to 184:20 when going from the low Z target carbon to the high Z target tungsten a drastic increase of reflected neon particles can be expected. Calculations performed with the TRIM-code [7] show an increase of the particle reflection coefficient R_N of neon ions, impinging with energies of 500 eV and angles of incidence of 60° typical for the experimental conditions considered, from 20% for the C-target to 68% for the W-target. The Doppler

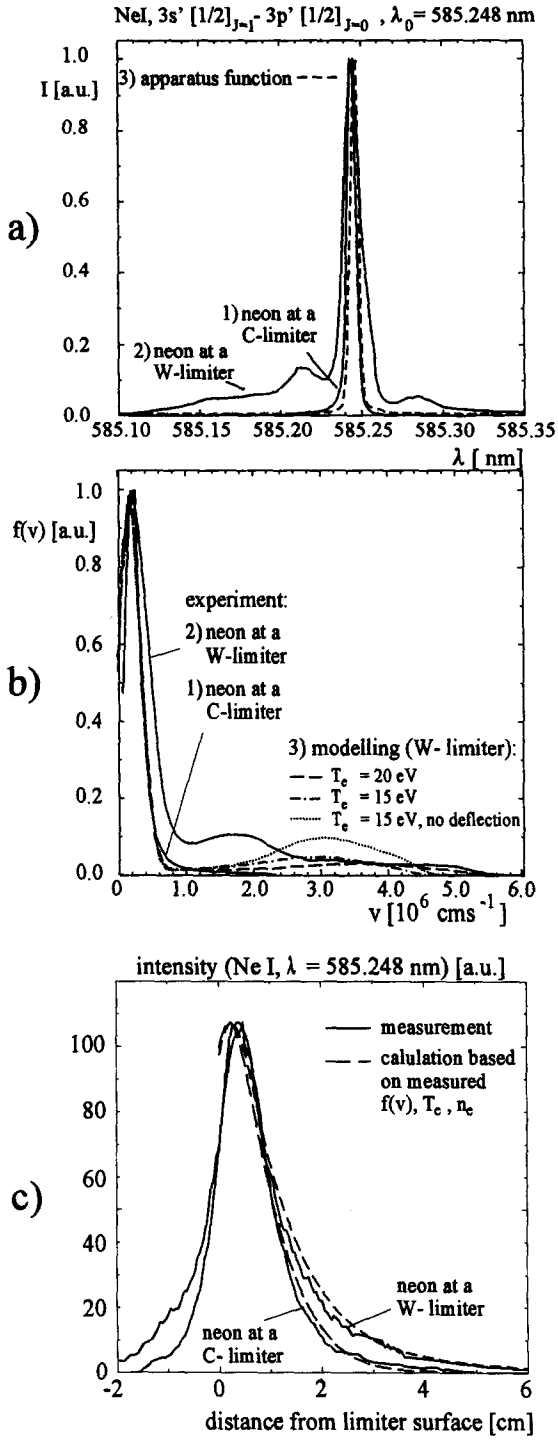

Fig. 2. (a) Doppler broadening of NeI line emission ($\lambda = 585.248$ nm): (1) carbon limiter, (2) tungsten limiter, (3) apparatus function, (b) velocity distribution of neon atoms: (1) carbon limiter, (2) tungsten limiter, (3) results from TRIM-calculations, (c) measured radial intensity distribution of NeI (solid lines) and calculations based on measured $f(v)$, $n_e(r)$ and $T_e(r)$ (dashed lines).

broadened emission profile of NeI at $\lambda = 585.248$ nm is depicted for both cases in Fig. 2a. In addition the spectrum of a neon glow discharge is shown, indicating the wavelength of atoms at rest and the apparatus function with a FWHM of 5×10^{-3} nm considered to unfold the spectra. The plasma background parameters are comparable in both discharges ($\bar{n}_e = 3.2 \times 10^{19}$ m^{-3}, local $T_e = 20$ eV, local $\bar{n}_e = 8 \times 10^{18}$ m^3, limiters located at the LCFS $r =$ 0.46 m). Both distributions consist of an intense central component attributed to the (ion induced) desorption of neon atoms with an energy of 0.35 eV and a wing of fast particles moving away from the limiter. The strongly increased number of fast particles seen in the blue wing of the neon spectrum at the W-limiter is apparent. The red wing seen here is due to reflection of light at the limiter surface and can be reproduced assuming a reflection coefficient of 30% for the W-surface. The velocity distributions deduced from the spectra are shown in Fig. 2b. The fraction of fast particles has been estimated by subtracting a Maxwellian velocity distribution with an energy of 0.35 eV from the measured ones. It increases from $15 \pm 5\%$ for the carbon limiter to $65 \pm 5\%$ for the tungsten limiter. The error was estimated from the uncertainty in determining the background of the spectra.

The experimental velocity distributions have been compared with calculations based on the TRIM-code modeling the reflection process and a Monte-Carlo code to take into account the detection probability of atoms in the observation volume for realistic geometry and plasma background [6]. Complete recycling at the limiter surface has been assumed: neon ions hitting the limiter are either reflected with the probability R_N and a certain energy loss (both calculated by TRIM) or desorbed with low energy ($E =$ 0.35 eV). The neon distribution at the carbon limiter is dominated by the thermal component. For the tungsten limiter we notice an excess of measured particles with velocities around $1.5–2.0 \times 10^6$ cm s^{-1} compared to the calculation. It has been impossible to overcome this discrepancy by changing those input parameters sensitive for reflection (the energy of neon ions hitting the limiter, which is determined by the plasma edge temperature, and their angle of incidence with respect to the surface normal, which is lowered by the acceleration of ions in the Debye sheath compared to the angle of incidence for the magnetic field lines). Fig. 2b shows the effect of an energy reduction of 25% and an increase of the angle of incidence to the value given by the intersection of the field lines in comparison to a parameter-set deduced from the experiment and model calculations with the RITM-code [8] ($T_e(a) =$ 20 eV, $T_i/T_e = 2$, averaged neon charge $\langle z_{Ne} \rangle = 5$, neon ion velocity equal to the deuterium sound velocity resulting in energies of about 500 eV as mentioned above). We conclude that the description with two components, a slow one from desorbed particles and a reflected one calculated by TRIM, is incomplete compared to the experimental results. This result confirms earlier results reported on recycling of neon at a carbon limiter for higher plasma densities and lower edge temperatures [6].

In addition we have measured the radial intensity distribution of the NeI-line at $\lambda = 585.248$ nm. This measurement characterizes the penetration of neon atoms into the confined volume and is shown in Fig. 2c. Based on the measured velocity distribution and measured n_e-/T_e-profiles we have calculated the intensity profile with the help of Eqs. (1) and (2). For both cases we find reasonable agreement between the measured and the calculated radial profile, giving an independent confirmation of the measured velocity distributions. The penetration depth of neon increases from 1.4 cm to 2.2 cm when going from the carbon to the tungsten case. This example illustrates the important influence of the velocity distribution of released neutrals governed by the PSI processes. A similar but even more pronounced effect has been seen when comparing the penetration depth of sputtered carbon and sublimated carbon [9].

5. Influence of local plasma parameters on the penetration depth of impurity neutrals and the neutral fueling efficiency

Variations of local n_e and T_e in front of the limiter have been produced by changing $\bar{n}_e$. An increase of the central density leads to a decrease of the penetration depth

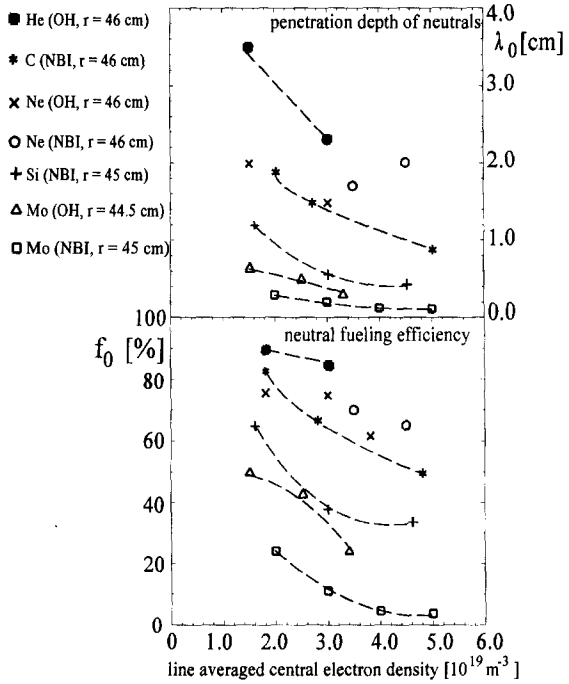

Fig. 3. Variation of penetration depths of impurity atoms inside the LCFS and neutral fueling efficiencies of He, C, Ne, Si and Mo with the line averaged central electron density (Ohmically and neutral beam heated discharges).

and of the fueling efficiency for species like carbon, silicon or molybdenum, where the ionization rate at the limiter increases and the averaged neutral velocity is independent of the local plasma parameters (e.g., for physically sputtered atoms) or decreases (as for carbon, where an increasing contribution of chemical erosion reduces the average velocity [9]). This effect is less prominent for species like helium and neon as the fraction of fast particles increases with higher densities due to an increasing reflection coefficient. Fig. 3 summarizes the penetration depths and neutral fueling efficiencies for different impurity species. The local plasma parameters vary from $n_e = 3\text{–}4 \cdot 10^{18}$ m^{-3}/$T_e = 60\text{–}80$ eV at the lowest central density shown to $n_e = 1.2\text{–}1.6 \cdot 10^{19}$ m^{-3}/$T_e = 15\text{–}30$ eV at the highest density for the neutral beam heated (NBI) cases, and $n_e = 1\text{–}2 \cdot 10^{18}$ m^{-3}/$T_e = 70$ eV to $n_e = 6 \cdot 10^{18}$ m^{-3}/$T_e = 20$ eV in Ohmic discharges. As both electron density and temperature at the LCFS increase when going from Ohmically to neutral beam heated plasmas for a given $\bar{n}_e$, the penetration depth and the neutral fueling efficiency decrease. For heavy impurities such as molybdenum the penetration depth and the neutral fueling efficiency are particularly small because of their small ionization potential and low velocity. More over, the prompt redeposition of ions at the surface within the first gyromotion is important because the penetration depth (see Fig. 3) is comparable to the gyroradius of Mo^+ (0.15 cm for an energy of 4 eV and a magnetic field of 1.8 T). The fraction of prompt redeposited molybdenum particles has been calculated from the radial ion source distribution for different $\bar{n}_e$ and is depicted in Fig. 4. The fraction increases from around 65 ∓ 5% at lowest densities to nearly 92 ∓ 5% at the highest densities observed, the error is caused by the uncertainty of the LCFS-position.

6. Link of edge processes to central impurity build-up

The next logical step is to link the measurements of the penetration of neutrals and the resulting ion source profiles to the central impurity densities. We will restrict ourselves to the comparison of relative variations when changing $\bar{n}_e$ as no absolute densities in the center have been available. Instead we use the intensity of L-shell emission of molybdenum (corrected for the variation of n_e/T_e, in the center determining the excitation rate of the emission lines [10] for a given density). These measurements are complemented by deposition rates of molybdenum collected by the collector probe in the SOL. As there is no direct connection with the test limiter along the field lines in the SOL, the deposition rates are a measure for the Mo-flux leaving the confined volume [1] (see Fig. 4). We have calculated the resulting central Mo-density with the proper Green's function using D, v and $\tau_{\|}$ as adjustable parameters [3]. The diffusion coefficient was assumed to be proportional to the edge temperature (Bohm-like) being 1.5 m^2 s^{-1} at the lowest $\bar{n}_e$. With respect to $\tau_{\|}$ in the SOL we distinguish between the parallel transport of ions born inside the LCFS and diffusing into the SOL (denoted as τ_1 and calculated as the ratio of connection length and ion sound velocity, being typically of the order 0.5 ms) and those ionized in the SOL and having a reduced parallel transport time τ_2 because they are flushed back to the limiter by the friction force of the background plasma [11]. Calculating the distance along the field lines the molybdenum ions can escape from the surface (see e.g. [12]) we estimate τ_2 to be one order of magnitude smaller than τ_1 at the lowest densities (smallest friction force) and two orders of magnitude smaller at the highest densities under investigation. The corresponding curves are shown in Fig.

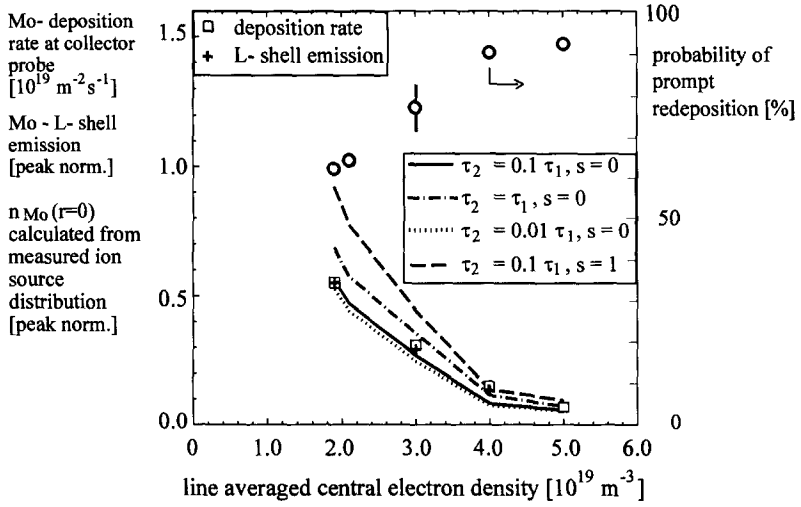

Fig. 4. Variation of the probability of prompt redeposition for molybdenum ions (circles), central molybdenum densities calculated with measured radial ion source distributions (lines), molybdenum deposition rates (boxes) and L-shell emission (crosses) with the line averaged central electron density (molybdenum test limiter at $r_{lim} = 0.45$ m, neutral beam heating with $P_{heat} = 1.6$ MW).

4. It is found that the absolute molybdenum densities do not vary strongly within these parameter variations. This can be explained by the fact that the amount of ionization processes taking place in the SOL and contributing to the central density is strongly reduced by prompt redeposition. Therefore, those atoms ionized inside the LCFS have the largest contribution to the central density. Introducing a moderate shaping factor $s = -v/D * a^2/r = 1$ (constant for all central densities) results in an increase of the central density of about 65% (see dashed curve in Fig. 4). The relative variation with increasing $\bar{n}_e$, is practically the same for all cases considered here and fits well to the reduction of the central density by a factor of 8 experimentally observed. Comparable results have been found for silicon release under neutral beam heated conditions [9].

7. Summary and conclusion

The penetration of impurity atoms into the plasma edge has been investigated with optical methods. The importance of the impurity release mechanism has been demonstrated comparing neon recycling at carbon and tungsten limiters where the penetration depth increases significantly in the latter case due to the larger number of fast reflected particles. The influence of n_e and T_e at the limiter radius has been shown for various impurity species, showing an increasing screening with increasing plasma density. This is most prominent for species whose velocities are not strongly affected by local n_e and T_e, e.g. for sputtered atoms. This screening is particularly effective for heavy species like molybdenum, where the penetration depth is so short, that prompt redeposition of ions within the first larmor orbit becomes important. For the release of molybdenum under neutral beam heated conditions it has been demonstrated that the variation of the central Mo-density can be explained satisfactorily by the variation of the molybdenum flux released from the limiter and the resulting ion source distribution with contributions from ionization inside and outside the LCFS. This result proves the importance of edge processes for the central impurity built-up.

References

[1] A. Pospieszczyk, in: eds. R.K. Janev and H.W. Darwin, Atomic and Plasma-Material Processes in Controlled Thermonuclear Fusion (Elsevier, Amsterdam, 1993) p. 213.
[2] W. Engelhardt and W. Feneberg, J. Nucl. Mater. 76–77 (1978) 518.
[3] G. Fussmann, Nucl. Fusion 26 (1986) 983.
[4] V. Philipps et al., Nucl. Fusion 34(11) (1994) 1417.
[5] B. Schweer et al., J. Nucl. Mater. 196–198 (1992) 174.
[6] B. Unterberg et al., J. Nucl. Mater. 196–198 (1995) 462.
[7] W. Eckstein and J.P. Biersack, Appl. Phys. A 38 (1985) 123.
[8] M. Tokar', Plasma Phys. Controlled Fusion 36 (1994) 1819.
[9] B. Unterberg et al., 22th EPS Conf. Bournemouth, Europhys. Abstr. 19C(II) (1995) 305.
[10] J. Rice et al., J. Phys. B 22 (1996) 2191.
[11] P.C. Stangeby and C. Farrell, Plasma Phys. Controlled Fusion 32 (1990) 677.
[12] P.C. Stangeby and I.D. Elder, J. Nucl. Mater. 220–222 (1995) 193.